A&A 448, 623–631 (2006)
DOI: 10.1051/0004-6361:20053603

Astronomy & Astrophysics

Extended envelopes around Galactic Cepheids

I. ℓ Carinae from near and mid-infrared interferometry with the VLTI

P. Kervella, A. Mérand, G. Perrin, and V. Coudé du Foresto

LESIA, UMR 8109, Observatoire de Paris-Meudon, 5 place Jules Janssen, 92195 Meudon Cedex, France
e-mail: Pierre.Kervella@obspm.fr

Received 9 June 2005 / Accepted 25 October 2005

ABSTRACT

We present the results of long-baseline interferometric observations of the bright southern Cepheid ℓ Carinae in the infrared N (8−13 μm) and K (2.0−2.4 μm) bands, using the MIDI and VINCI instruments of the VLT Interferometer. We resolve in the N band a large circumstellar envelope (CSE) that we model with a Gaussian of 3 $R_\star$ ($\approx$500 $R_\odot$ $\approx$ 2−3 AU) half width at half maximum. The signature of this envelope is also detected in our K band data as a deviation from a single limb darkened disk visibility function. The superimposition of a Gaussian CSE on the limb darkened disk model of the Cepheid star results in a significantly better fit of our VINCI data. The extracted CSE parameters in the K band are a half width at half maximum of 2 $R_\star$, comparable to the N band model, and a total brightness of 4% of the stellar photosphere. A possibility is that this CSE is linked to the relatively large mass loss rate of ℓ Car. Though its physical nature cannot be determined from our data, we discuss an analogy with the molecular envelopes of RV Tauri, red supergiants and Miras.

Key words. Cepheids – techniques: interferometric – stars: circumstellar matter – stars: individual: ℓ Car

1. Introduction

Cepheids are commonly used as distance indicators, thanks to their well-established Period-Luminosity (P–L) law. Discovered almost one century ago, this empirical relation relates the absolute brightness of a Cepheid to its variation period. Measuring the period and apparent brightness of a Cepheid thus gives its distance. As they are intrisically very bright stars, and can be observed in distant galaxies, this remarkable property has turned these yellow supergiant stars into primary standard candles for extragalactic distance estimations.

The calibration of the P–L zero point itself relies essentially on the Baade-Wesselink (BW) method. This classical method (Baade 1926; Wesselink 1946) establishes the distances to Cepheids by determining simultaneously the change in linear and angular size over the pulsation. The linear size change is obtained from an integration of spectrographic radial velocity measurements, while the change in angular size can be obtained either from surface brightness considerations (classical method) or directly by interferometry. One potential weakness of the BW technique is that it relies implicitely on the asumption that the star radiates as a blackbody (surface brightness method) or can be resolved directly as a single, "naked" star (interferometric BW method). A deviation from these hypotheses, caused for instance by the presence of a circumstellar envelope (CSE), can lead to a bias in the resulting distance estimation.

We present here an interferometric investigation of the close environment of the bright southern Cepheid ℓ Car (HD 84810, HR 3884). As it is the brightest Cepheid in the sky, it was extensively studied using a variety of techniques. For instance, applications of the classical and interferometric BW method to this star can be found in Taylor et al. (1997) and Kervella et al. (2004c). We present in Sect. 2 our interferometric observations that were obtained using the VINCI and MIDI instruments of the VLTI. Section 3 is dedicated to the interpretation of the measured visibilities in terms of simple flux distribution models. In Sects. 4 and 5, we discuss the different physical processes that are likely to play a role in the formation of a CSE around ℓ Car, and we compare it to two variable star classes related to Cepheids (RV Tauri and Miras) that are known to host dusty environments.

2. Observations

2.1. VINCI

2.1.1. Raw data acquisition and processing

The European Southern Observatory's Very Large Telescope Interferometer (VLTI; Glindemann et al. 2004) has been operated on top of the Cerro Paranal, in Northern Chile since March 2001. For the new observations reported in this paper, the light coming from two test siderostats (0.35 m aperture) or two 8 m Unit Telescopes (UTs) was recombined coherently

in VINCI, the VLT INterferometer Commissioning Instrument (Kervella et al. 2000; Kervella et al. 2003). We used a regular K band filter ($\lambda = 2.0-2.4$ μm), and processed the data using the standard VINCI data reduction software version 3.0 (Kervella et al. 2004a). As part of our programme of Cepheid observations by interferometry, we have observed ℓ Car in January-February and April-May 2003. These measurements, obtained using the VLTI test siderostats on the B3-M0 baseline (140 m ground length, ≈125 m projected on the sky), were already reported in Kervella et al. (2004b, hereafter Paper I).

During the early VLTI commissioning (Jan.−Feb. 2002), additional visibility measurements of ℓ Car were obtained using the 8 m Unit Telescopes UT1 and UT3 (102 m ground length, ≈85 m projected), and with the test siderostats on the short E0-G0 baseline (16 m ground length, ≈14.5 m projected). The Unit Telescopes were not equipped at the time with adaptive optics systems (seeing limited regime). These new data are listed in Tables 1 and 2. The reference Julian date epoch (T_0 = 2 452 290.4158) and pulsation period (P = 35.551341 days) used to compute the phase are taken from Szabados (1989), and are identical to Paper I. The calibrators were chosen from the Cohen et al. (1999) catalogue (Table 3). As demonstrated by Bordé et al. (2002), the star diameters in this list have been estimated homogeneously to a relative precision of 1% and agree well with other angular diameter estimation methods.

2.1.2. Medium vs. long baselines: a discrepancy?

A first indication that a simple stellar disk model is not the most adequate for ℓ Car comes from the comparison of the observations obtained using the medium (UT1-UT3, ≈85 m) and long (B3-M0, ≈125 m) baselines. In order to derive angular diameters from the VINCI visibilities, we used the limb darkening model from Claret (2000), in the same way as described in Paper I. Figure 1 shows the evolution of the limb darkened angular diameter of ℓ Car as a function of phase. The solid curve is the result of the fit of the integrated radial velocity curve of this star to the B3-M0 data only (as described in Paper I). It appears clearly that the new angular diameter measurements from the UT1-UT3 baseline, represented as open squares, are larger by 3σ than those obtained with the siderostats.

We now examine the possible calibration or instrumental causes for this difference. It is improbable that it comes from an incorrect estimation of the angular diameter of the calibrators, as two different reference stars were used for the UT measurements (HR 4080 for phase 0.376 and HR 4831 for phase 0.490), with consistent results. Moreover, HR 4831 was also used for part of the siderostat observations (Table 2) with no detectable bias compared to other calibrators. The calibrators were all chosen from the catalogue by Bordé et al. (2002). This is a filtered version of the reference work by Cohen et al. (1999) that was adapted specifically for interferometry. All these calibrators are believed to be single stars, and do not show infrared excess.

It is also unlikely that a systematically different behavior between the siderostats and the UTs can create such a difference. Firstly, previous observations demonstrated a good agreement between these two types of light collectors for well-known stars (see e.g. Di Folco et al. 2004). Secondly, the visibility measurements being differential in nature (between the Cepheid and its calibrator), the existence of a "telescope type" bias would require a differential effect between the star and its calibrator. This is unlikely as the brightness and colors are chosen to be similar. The main difference between UTs and siderostats is the pupil size (8 m vs. 0.35 m). The field of view coupled in the single-mode fibers is 1.5″ with the siderostats (i.e. limited by the diffraction), and of the order of 1″ with the UTs in the K band (limited by the atmospheric seeing, see Guyon 2002 for details). Given the characteristic size of the

Table 1. Squared visibilities of ℓ Car in the K band from VINCI. The stations of the new measurements are marked in bold characters. The calibrators are given in italic characters. The stated Julian date JD_0 is JD−2.452 10^6. The azimuth is counted in degrees clockwise from North (N = 0 deg, E = 90 deg), and B is the projected baseline in meters. The pulsation phase ϕ is computed using the P and T_0 parameters from Szabados (1989).

JD_0	ϕ	B (m)	Az.	$V^2 \pm$ stat $\pm$ syst (%)
E0-G0				*HR 4546*
792.486	0.122	14.560	19.03	95.32 ± 3.97 ± 0.05
792.499	0.123	14.308	21.32	98.82 ± 3.68 ± 0.05
792.545	0.124	13.316	27.30	93.28 ± 3.91 ± 0.05
792.576	0.125	12.644	29.50	99.20 ± 6.14 ± 0.04
792.582	0.125	12.533	29.74	102.08 ± 6.63 ± 0.04
792.587	0.125	12.433	29.94	94.12 ± 6.53 ± 0.04
793.544	0.152	13.287	27.42	97.95 ± 2.83 ± 0.04
793.555	0.152	13.048	28.32	97.24 ± 2.68 ± 0.04
793.560	0.153	12.930	28.71	95.72 ± 2.75 ± 0.04
B3-M0				*HR 4546*
765.523	0.364	125.951	75.96	9.64 ± 0.41 ± 0.49
765.528	0.364	125.063	77.50	10.89 ± 0.54 ± 0.55
765.534	0.364	124.029	79.24	11.46 ± 0.72 ± 0.58
765.575	0.365	115.637	91.95	16.57 ± 0.63 ± 0.85
765.580	0.366	114.483	93.59	18.73 ± 1.68 ± 0.96
765.588	0.366	112.611	96.21	17.62 ± 0.46 ± 0.91
U1-U3				*HR 4080*
303.772	0.376	84.682	45.25	38.28 ± 0.73 ± 0.28
303.775	0.376	84.399	45.81	38.80 ± 0.78 ± 0.28
303.776	0.376	84.254	46.10	40.13 ± 0.86 ± 0.29
303.778	0.376	84.023	46.55	37.58 ± 0.72 ± 0.27
B3-M0				*HR 4546*
766.516	0.392	126.748	74.53	9.52 ± 0.50 ± 0.49
766.521	0.392	125.889	76.07	12.08 ± 0.86 ± 0.62
766.526	0.392	125.045	77.53	11.36 ± 0.94 ± 0.58
766.544	0.393	121.582	83.16	12.24 ± 0.45 ± 0.62
766.576	0.394	114.779	93.17	16.23 ± 0.56 ± 0.80
766.581	0.394	113.604	94.82	17.47 ± 0.63 ± 0.86
766.586	0.394	112.390	96.52	17.72 ± 0.66 ± 0.87

Table 2. Continued from Table 1.

JD_0	ϕ	B (m)	Az.	$V^2 \pm$ stat $\pm$ syst (%)
B3-M0				*HR 4546*
768.523	0.448	124.548	78.38	11.66 ± 0.50 ± 0.58
768.528	0.448	123.683	79.81	13.28 ± 1.31 ± 0.66
768.536	0.449	122.082	82.38	12.85 ± 1.59 ± 0.64
768.581	0.450	112.204	96.78	18.42 ± 0.55 ± 0.81
768.591	0.450	109.878	100.01	19.75 ± 0.52 ± 0.87
768.599	0.450	107.804	102.89	21.07 ± 0.60 ± 0.93
768.607	0.451	105.748	105.77	23.35 ± 0.60 ± 1.03
B3-M0				*HR 3046, HR 4831*
769.570	0.478	114.286	93.86	17.31 ± 0.69 ± 0.27
769.574	0.478	113.127	95.49	17.83 ± 0.75 ± 0.27
769.580	0.478	111.834	97.29	18.66 ± 0.74 ± 0.29
U1-U3				*HR 4831*
307.822	0.490	75.924	59.76	46.98 ± 1.06 ± 0.35
307.823	0.490	75.666	60.12	47.33 ± 0.88 ± 0.35
307.825	0.490	75.342	60.58	47.26 ± 0.84 ± 0.35
307.827	0.490	74.989	61.07	48.13 ± 0.91 ± 0.36
B3-M0				*HR 3046, HR 4831*
770.533	0.505	121.671	83.02	13.30 ± 0.56 ± 0.18
770.538	0.505	120.634	84.62	14.24 ± 0.61 ± 0.20

source of a few mas, this small difference cannot be the cause of a significant bias.

This systematic difference between the visibility data obtained on the B3-M0 and UT1-UT3 baselines is therefore unlikely to have an instrumental origin. In Sect. 3, we present a model of ℓ Car surrounded by a circumstellar environment (CSE) that can reproduce the data from both medium and long baselines, as well as the shorter (≈14.5 m projected) E0-G0 data.

2.2. MIDI

2.2.1. Raw data acquisition and processing

The MIDI observations of ℓ Car were obtained on the night of 8−9 April 2004, using the UT2-UT3 baseline of the VLTI. This baseline has a ground length of 46.6 m, but due to the low declination of ℓ Car and its calibrator, the projected baseline was 40.0 m. The raw data were processed using the MIDI Data Reduction Software developed by the Paris Observatory and distributed by the JMMC[1] in order to extract first the instrumental squared coherence factors and then the calibrated squared visibilities $V^2(\lambda)$. As MIDI operates in the diffraction limited regime of the UTs, the effective field of view diameter is equal to approximately 0.26″ at $\lambda = 10\,\mu$m. This is much larger than the typical angular size of the star and of its CSE (≈10 mas) discussed in Sect. 3. Perrin et al. (2005b) describe the steps to calibrate the MIDI data carried out by the software. This software also outputs the spectra of the source and calibrator over the N band. The presence of a strong ozone atmospheric absorption band over the range $\lambda = 9.3{-}10.0\,\mu$m (Lord 1992) can make the visibilities unreliable in this wavelength domain, as the photometric calibration is made more difficult by the lower flux level.

[1] Jean-Marie Mariotti Center (`http://mariotti.fr`).

2.2.2. Spectral energy distribution

The absolutely calibrated spectrum of ℓ Car presented in Fig. 2 was obtained by dividing the average observed with MIDI by the average spectrum of its calibrator HR 3187, and then multiplying the result by the absolutely calibrated template spectrum of HR 3187 given by Cohen et al. (1999). The agreement with the IRAS spectrum obtained on this star (Volk & Cohen 1989) is satisfactory. At the date of the MIDI observations (JD = 2 453 104.6), the pulsation phase of ℓ Car was $\phi = 0.901$: the star was just starting its inflation phase, shortly after its minimum diameter ($\phi = 0.89$).

While ℓ Car is rising towards maximum light in the visible ($\phi = 1.00$ by definition), it is almost at minimum light in the K band. Using the temperature scale from Kiss & Szàtmary (1998), with $B - V$ photometry and the color excess from Fernie (1990), we derive $T_{\rm eff} = 5500$ K for phase 0.901. Together with the extrapolated VINCI LD angular diameter for this phase ($\theta_{\rm LD} \simeq 2.70$ mas), we obtain the blackbody spectrum represented as a solid curve in Fig. 2. It is in excellent agreement with the IRAS observations, as well as with the MIDI spectrum. In the infrared, the photometry of a Cepheid is essentially determined by its change in apparent size, as opposed to the visible where its effective temperature plays the leading role. For instance, the amplitude of the photometric variation of ℓ Car in the K band is $\Delta m_K = 0.32$, corresponding to a ≃16% amplitude in terms of angular size. This is consistent with the pulsation amplitude of 18% measured with VINCI (Paper I). The small remaining difference between the IRAS and MIDI spectra can be explained by a pulsational variation of the radius of ℓ Car between the two observations. Unfortunately, the date at which the IRAS spectra were obtained is not available in the IRAS LRS catalogue, and we cannot compute the phase to check this hypothesis.

2.2.3. Calibration

The calibrator star used for the MIDI observations, HR 3187, was selected from the Cohen et al. (1999) catalogue, as the VINCI calibrators. This star is unresolved by the interferometer at the wavelengths sampled by MIDI (8−13 μm), with an angular diameter of only 2.4 mas (Table 3).

Figure 3 shows the result of the calibration of the ℓ Car observations using two different calibration hypotheses. In this figure, *Cal1* and *Cal2* refer to the first and second series of observations of HR 3187, while *Sci1* and *Sci2* refer to the first and second series of ℓ Car (Table 4). The first hypothesis is to consider the average transfer function (TF) of the interferometer over all calibrator observations, and apply it to all observations of ℓ Car. In the second case, *Cal1* is associated with *Sci1* and *Cal2* with *Sci2*. These two calibration choices

Table 3. Relevant parameters of the calibrators of ℓ Car (F6Ib-K0Ib), taken from Bordé et al. (2002).

HR	HD	m_V	m_K	m_N	Sp. Type	$T_{\rm eff}$(K)	$\log g$	π (mas)[a]	$\theta_{\rm LD}$(mas)[b]	$\theta_{\rm UD\,K}$(mas)[c]
HR 3046	HD 63744	4.70	2.31	2.42	K0III	4720	2.6	14.36 ± 0.48	1.67 ± 0.025	1.63 ± 0.024
HR 3187	HD 67582	5.04	2.04	2.24	K3III	4250	2.4	2.63 ± 0.51	2.39 ± 0.062	2.32 ± 0.061
HR 4080	HD 89998	4.83	2.40	2.44	K1III	4580	2.5	16.26 ± 0.56	1.72 ± 0.020	1.68 ± 0.019
HR 4546	HD 102964	4.47	1.56	1.67	K3III	4210	2.2	7.03 ± 0.72	2.48 ± 0.036[d]	2.41 ± 0.035[d]
HR 4831	HD 110458	4.67	2.28	2.39	K0III	4720	2.6	17.31 ± 0.65	1.70 ± 0.018	1.66 ± 0.018

[a] Parallaxes from the HIPPARCOS catalogue (Perryman et al. 1997).
[b] Catalogue values from Cohen et al. (1999).
[c] Linear limb darkening coefficients factors from Claret et al. (1995).
[d] The angular diameter of HR 4546 has been measured separately with VINCI.

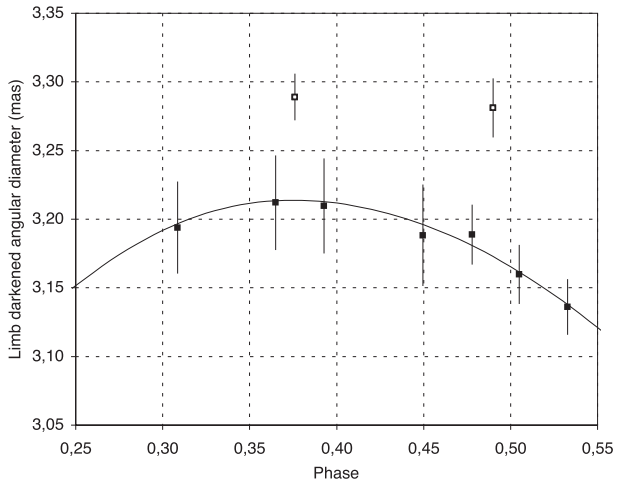

Fig. 1. Limb darkened disk angular diameter of ℓ Car deduced from VINCI observations on the B3-M0 siderostat baseline (filled squares) and the UT1-UT3 baseline (open squares). The solid curve is the best-fit model from Paper I, using the siderostat data only.

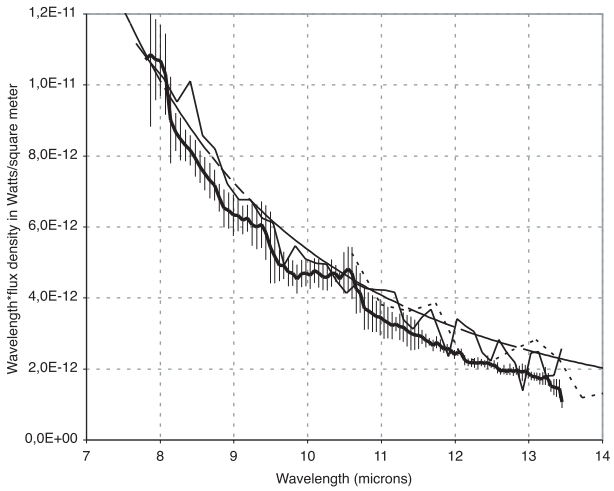

Fig. 2. Absolutely calibrated MIDI (thick curve) and IRAS LRS spectra (thin solid and dotted curves) of ℓ Car, using HR 3187 as a spectrophotometric standard star. The theoretical spectrum of a blackbody with $T = 5500$ K and an angular diameter of 2.70 mas is superimposed for reference (solid curve).

simply result in a vertical shift of the $V^2(\lambda)$ spectrum, leaving its shape qualitatively the same (rising from short to long wavelengths). This shows that independent of the calibration hypothesis, ℓ Car is significantly resolved by the interferometer. In the following, we have chosen to keep the association *Cal1-Sci1* and *Cal2-Sci2*, as the target and calibrator observations are slightly closer in time in this case. Qualitatively, the choice of the first hypothesis (average TF over the night) would have resulted in slightly lower visibilities, meaning that the object would appear even more resolved.

3. Model fitting

3.1. K band model

We model the visibility curve using a limb darkened disk (LD) representing the star, and a superimposed Gaussian shape representing the CSE. The stellar disk has only one parameter, the LD angular diameter ($\theta_{\rm LD}$), while the Gaussian shape has a variable full width at half maximum (FWHM) $D_{\rm CSE\,K}$ and total intensity $I_{\rm CSE\,K}$, normalized to the stellar brightness at center. The limb darkening profile for the star is taken from Claret (2000), considering the physical parameters of ℓ Car detailed in Paper I ($T_{\rm eff}$, $\log g$, ...). The visibility model is computed taking into account the bandwidth smearing effect (Davis et al. 2000; Kervella et al. 2004a) that is due to the broadband operation of VINCI. This is one of the simplest models to account for the contribution of a diffuse CSE, together with the photospheric emission from the star itself. Radiative transfer is not modeled at this stage. The model is purely geometric to ease the interpretation of the measured visibility points. The resulting $V^2(D_{\rm CSE\,K}, I_{\rm CSE\,K}, B)$ model is adjusted numerically to the observed $(B, V^2)_i$ data using a classical χ^2 minimization process. Figures 4 and 5 show the best fit model to the VINCI data.

For this fitting process, we considered only the VINCI measurements obtained between phases 0.36 and 0.51 on the B3-M0 baseline (≈125 m). We limited our selection to this range as it covers the phases of the intermediate baseline observations with the UTs. This way, we can separate the pulsation of the star from the presence of a CSE, and study the spatial light distribution of the star for a given phase of its pulsation. The data obtained on the E0-G0 baseline (≈14.5 m) are

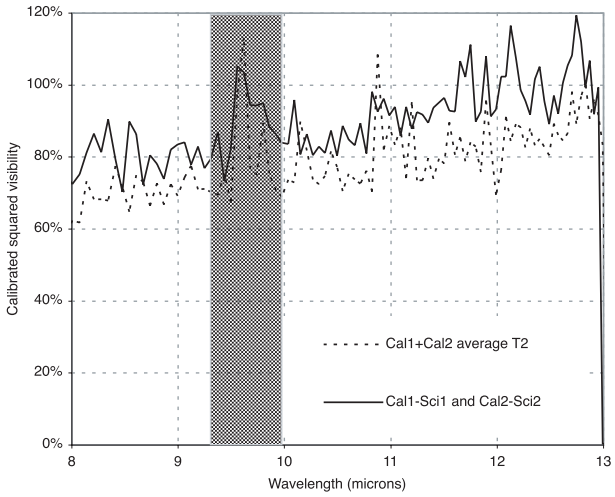

Fig. 3. Result of different calibration hypotheses for ℓ Car (see text for explanation). The shaded area corresponds to an atmospheric absorption feature of ozone ($\lambda = 9.3-10.0\,\mu$m, Lord 1992), where the data can be unreliable.

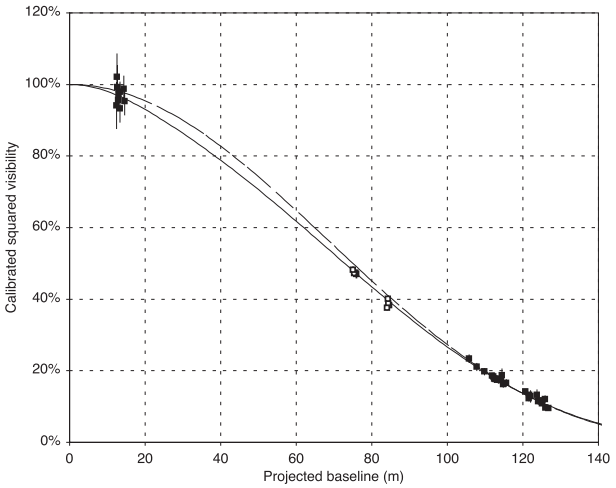

Fig. 4. Observed squared visibilities of ℓ Car with VINCI, and best fit model composed of a Gaussian CSE superimposed on a limb darkened disk (solid curve). The dashed curve is a simple uniform disk model fit to the B3-M0 siderostat data only (longest baseline). The data obtained with the UTs are marked with open squares, while the siderostat data are represented by filled squares.

Table 4. Journal of MIDI observations of ℓ Car on the UT2-UT3 baseline. JD_1 is defined as JD−2 453 104 (pulsation phase $\phi = 0.901$). B is the projected baseline length, Alt. the altitude of the star and PA is the position angle of the projected baseline ($N = 0°$, $E = 90°$).

UTC	JD_1	Target	Alt. (°)	B (m)	PA (°)
01:25:47	0.559	ℓ Car	52.07	40.85	48.52
01:26:40	0.560	ℓ Car	52.07	40.82	48.68
01:27:33	0.561	ℓ Car	52.07	40.79	48.84
01:48:28	0.575	HR 3187*	56.60	38.95	58.75
01:49:21	0.576	HR 3187	56.60	38.89	58.85
01:50:14	0.577	HR 3187	56.60	38.83	58.95
02:08:35	0.589	ℓ Car	51.11	39.22	56.25
02:09:28	0.590	ℓ Car	51.11	39.18	56.41
02:10:21	0.591	ℓ Car	51.11	39.14	56.57
02:28:55	0.603	HR 3187	49.98	35.92	63.40
02:29:48	0.604	HR 3187	49.98	35.85	63.50
02:30:41	0.605	HR 3187	49.98	35.78	63.60

* These data show a deficit in terms of photometry, and were not used in the calibration process.

not affected by the pulsation phase, as the K band photosphere remains largely unresolved on this short baseline ($V^2 \simeq 98\%$), and these data are thus sensitive only to extended emission.

We obtain the model parameters listed in Table 5. In terms of stellar radii, the CSE reaches $R_{\mathrm{CSE\,K}} = 1.9 \pm 1.4\ R_\star$ or $330 \pm 270\ R_\odot$, in the K band (assuming $R_\star = 179\,R_\odot$ from Kervella et al. 2004c). The large uncertainty on this radius is due to the relative lack of interferometric data for baselines between 15 and 75 m. The main constraint is the deficit, in term of visibilities, at baselines between 75 and 85 m. The total brightness of this environment represents 4% of the stellar brightness. The LD size of ℓ Car considering only the B3-M0 baseline measurements is $\theta_{\mathrm{LD}} = 3.093 \pm 0.009$ mas, only 0.6% away in terms of angular diameter from the best fit model with a CSE. Therefore, the results in terms of average diameter and distance reported by Kervella et al. (2004c) are not modified by the presence of this CSE.

3.2. N band model

From the VINCI observations in the K band reported in Paper I, we know that the angular diameter of the star at pulsation phase $\phi = 0.901$ is $\theta_{\mathrm{LD}} \simeq 2.70$ mas. This is beyond the resolution capabilities of MIDI on the UT2-UT3 baseline, and the squared visibility spectrum $V^2(\lambda)$ should therefore appear as the thin solid curve in Fig. 6 (top). The presence of a significant slope and squared visibilities as low as 80% at $\lambda = 8\,\mu$m however shows that a CSE is resolved by the interferometer.

Fitting the data with a Gaussian model results in an average FWHM of $D_{\mathrm{CSE\,N}} = 8 \pm 3$ mas. In this fitting process, the error bars of each $V^2(\lambda)$ value were not averaged, as it is currently not possible to separate the systematic and statistical contributions to these errors. We therefore chose this conservative approach to avoid underestimating the final error bars. The apparent size of the CSE appears to vary slightly over the N band, with a maximum size between 8 and 11 μm.

While the CSE appears to be relatively faint in the K band, it becomes much more visible in the N band, even dominating the star itself. The typical size of the CSE is similar in the two bands with a half FWHM of about $2-3\ R_\star$.

4. Nature of the CSE of ℓ Car

4.1. Circumstellar matter

Only one Cepheid is currently known to be associated with a CSE, RS Pup. Another Cepheid, SU Cas, appears to be located

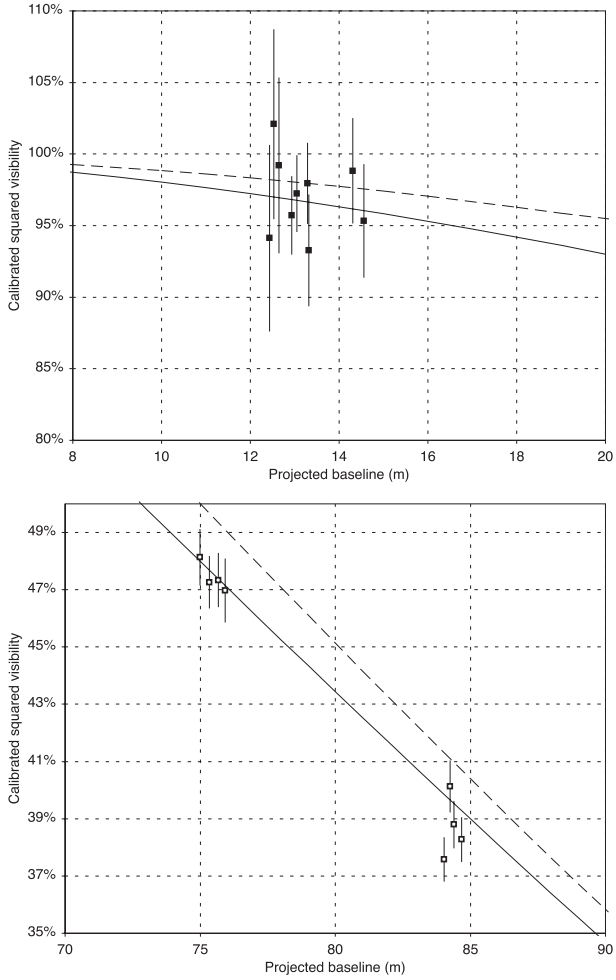

Fig. 5. Enlargements of Fig. 4 showing the squared visibility measurements obtained. *Top*: short E0-G0 siderostat baseline. *Bottom*: intermediate UT1-UT3 baseline.

Table 5. Best fit model parameters for the VINCI data in the K band. The adjusted model is the superimposition of a limb darkened disk representing the stellar photosphere and a Gaussian representing a CSE. $\theta_{\rm LD}$ is the LD angular diameter of the star, $D_{\rm CSE\,K}$ is the FWHM of the Gaussian (in mas), and $I_{\rm CSE\,K}$ is the ratio of the CSE brightness to the stellar brightness in the K band.

$\theta_{\rm LD}$ (mas)	$D_{\rm CSE\,K}$ (mas)	$I_{\rm CSE\,K}$	Reduced χ^2
3.11 ± 0.03	5.8 ± 4.5	$4.2 \pm 0.2\%$	0.65

close to a nebula, but the association is uncertain. The mechanism for the formation of the RS Pup shells is currently unknown. Deasy (1988) has proposed several scenarios, ranging from an evolution of the star before its Cepheid phase to mass loss during multiple crossings of the instability strip. As pointed out by Havlen (1972) and Szabados (2003), it is unlikely that RS Pup is the only existing Cepheid-nebula association. The detection of such nebulae is made particularly difficult by the large intrinsic brightness of the Cepheids themselves. They are extremely bright supergiants, and therefore they largely outshine their close environment, including possible associated nebulae.

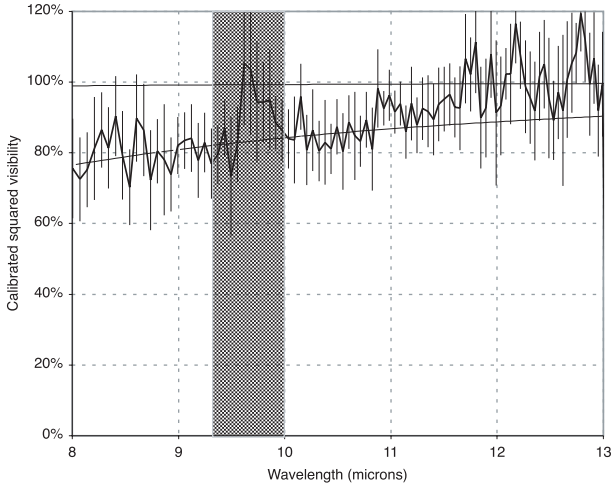

Fig. 6. Calibrated squared visibility $V^2(\lambda)$ of ℓ Car using the UT2-UT3 baseline (40 m projected length). The dashed curve is the best fit Gaussian model with a FWHM of $r_{\rm CSE}(N) = 8 \pm 3$ mas. The thin, almost linear solid curve close to 100% represents the visibility function of the K band photosphere of ℓ Car ($\theta_{\rm LD} = 2.70$ mas), at the phase of the MIDI observations ($\phi = 0.901$).

4.2. Mass loss

Based on IRAS photometry and IUE ultraviolet spectra, Deasy (1988) has identified mass loss in a number of Cepheids. The highest mass loss is attributed by this author to RS Pup ($10^{-6}\,M_\odot\,{\rm yr}^{-1}$). This level is very significant, and explains the "bubble" structures that have been carved by this star in the interstellar medium. ζ Gem is also quoted as exhibiting evidence of stellar wind in its ultraviolet spectra, inducing a mass loss of $\simeq 10^{-10}\ M_\odot\,{\rm yr}^{-1}$, several magnitudes smaller than RS Pup. ℓ Car shows also a significant mass loss, with a rate about three times as large as ζ Gem. Böhm-Vitense & Love (1994) even obtained a much higher value of $\simeq 2 \times 10^{-5}\ M_\odot\,{\rm yr}^{-1}$ for this star, even larger than RS Pup. They suggest that the fixed (non pulsating) Hα absorption feature that they detect is caused by a CSE with a size of the order of 1000 AU. At the distance of ℓ Car (570 pc, Kervella et al. 2004c), this corresponds to an angular extension of $0.5''$. In addition, they detect "blobs" of OI emission up to a distance of several arcseconds from the star. The MIDI observations are sensitive to the central, hotter part of this CSE. Finally, these authors suggest in their conclusions that the mass loss rate may be larger for long period Cepheids than for short periods. This is also the conclusion of Willson (1988) based on theoretical pulsation computations: larger mass stars are associated with more mass loss: ℓ Car, with $P = 35.5$ days, is thus a prime candidate for a bright CSE.

4.3. Infrared excess

A number of Cepheids have shown moderate infrared excesses that are related to the presence of circumstellar matter. An excessive brightness at mid-infrared wavelengths is characteristic of a relatively warm, dusty environment. Deasy (1988) compared the IRAS excess ratios $F(60\,\mu{\rm m})/F(12\,\mu{\rm m})$ to predicted values for several bright Cepheids. Interestingly, an

extended infrared emission is identified around X Pup, located only $\simeq$1 kpc from RS Pup, and probably associated with the same nebula. Using IRAS data in the mid-IR, McAlary & Welch (1986) have studied a broad sample of Cepheids in order to detect infrared excesses. They obtained a clear detection in the case of RS Pup and SU Cas (two classical Cepheids). For ℓ Car however, we confirm their conclusion that no significant mid-IR excess is present in ℓ Car from our N band spectrum presented in Sect. 2.2.2.

Depending on its composition and temperature, the contribution from the CSE in the mid-IR could be small, especially as it may essentially diffuse the K band light from the star itself. Such a limited excess may well have remained below the sensitivity limit of the photometric detection methods. Moreover, this IR excess could be variable due to the change in effective temperature of the star, and the propagation of shock waves in the CSE around the minimum diameter phase. A cold temperature could for instance result in an excess at even longer wavelengths than the mid-infrared sampled with MIDI, up to the millimetric domain. No IR excess has been found with IRAS down to 60 μm, but Cepheids have never been studied at longer wavelengths.

The Gaussian model that we use in Sect. 3 for the CSE of ℓ Car should not be considered as physically realistic. In particular, it is clear that dust cannot exist within several radii of the star itself, as it would be sublimated. Nevertheless, we have chosen this simplified distribution in order to fit our limited data set with the smallest possible number of parameters. In order to establish the true geometry of the CSE, we plan to obtain in the future more visibility measurements over a broader range of spatial frequencies, as well as closure phases to search for deviations from central symmetry.

4.4. Polarization

Bastien et al. (1988) measured a significant fraction of polarized flux on ℓ Car with 1.58 ± 0.01% in the visible, at a position angle of 99.8 ± 0.2 deg. These authors noted that this polarization level is exactly the same as what was found by Serkowski, Matthewson & Ford (1975), 18 years before. A quick search through the catalogue compiled by Heiles (2000) reveals that several nearby Cepheids show a significant level of polarization (Table 6). Some fainter Cepheids located further away are known to present larger polarizations, but the fraction of the polarization introduced by the interstellar dust becomes uncertain.

Polyakova (1990) proposed that the observed polarization of Cepheids may be caused by the presence of a CSE that is 20 to 30% larger in the equatorial direction than along its pole. It would be interesting to measure interferometrically the shape of the CSE, using for instance the AMBER instrument (Petrov et al. 2000) to test this hypothesis.

Table 6. Fraction of polarized flux (p) for bright Cepheids. This list is limited to Cepheids brighter than $m_V = 6.0$ at maximum present in the catalogue assembled by Heiles (2000), apart from RS Pup. The color excess $E(B-V)$ reported by Fernie (1990) is given for each star, and the p values larger than 1% are marked in bold characters.

Star	m_V	$E(B-V)$	$p \pm \sigma(p)$ (%)
FF Aql	5.2	0.22	0.620 ± 0.006
η Aql	3.5	0.15	$\mathbf{1.685 \pm 0.003}$
RT Aur	5.0	0.05	0.490 ± 0.120
U Car	5.7	0.28	0.560 ± 0.100
v382 Car	3.8	–	0.510 ± 0.100
v399 Car	4.6	–	$\mathbf{1.425 \pm 0.090}$
ℓ Car*	3.3	0.17	$\mathbf{1.580 \pm 0.010}$
SU Cas	5.7	0.29	$\mathbf{1.853 \pm 0.036}$
δ Cep	3.5	0.09	0.440 ± 0.083
BG Cru	5.3	0.05	0.660 ± 0.035
X Cyg	5.8	0.29	0.410 ± 0.120
DT Cyg	5.6	0.04	0.280 ± 0.120
β Dor	3.5	0.04	0.440 ± 0.035
ζ Gem	3.6	0.02	0.110 ± 0.100
ω Gem	5.1	–	0.090 ± 0.120
T Mon	5.6	0.21	0.320 ± 0.120
Y Oph	5.9	0.66	$\mathbf{1.340 \pm 0.120}$
MY Pup	5.5	0.06	0.400 ± 0.035
RS Pup	7.0	0.45	0.440 ± 0.100
S Sge	5.2	0.13	0.689 ± 0.009
W Sgr	4.3	0.11	0.775 ± 0.016
X Sgr	4.2	0.20	$\mathbf{1.708 \pm 0.232}$
Y Sgr	5.2	0.21	0.220 ± 0.120
AH Vel	5.5	0.07	0.100 ± 0.100
T Vul	5.4	0.06	0.220 ± 0.120

* The value of p for ℓ Car is taken from Bastien et al. (1988).

5. Envelopes around stars related to Cepheids

5.1. The RV Tauri star AC Her

According to the General Catalogue of Variable Stars (Kholopov et al. 1998), variables of the RV Tauri class are pulsating yellow supergiants having spectral types F-G at maximum visible light and K-M at minimum. Their light curve shows alternating deep and shallow minima with a period (measured between one deep minimum and the next) of 30 to 150 days and an amplitude of 3 to 4 mag in the visible. RV Tau stars are particularly interesting as they seem to be intermediates between Cepheids and Mira variables. They are included in the broad group of "Type II Cepheids" (Wallerstein 2004). They are generally surrounded by dust shells that have been studied by several authors, including for instance Gherz (1972) and Jura (1986). On the theoretical side, Moskalik & Buchler (1991) have shown that an RV Tau-like pulsational behavior can be observed in long period Cepheids ($P = 25$–40 days), based on numerical models of Cepheids.

Shenton et al. (1992) have analyzed multi-wavelength photometry and spectroscopy of the short period RV Tauri star AC Her, from the ultraviolet to the infrared. This star is especially interesting as it pulsates with a very regular "double period" of 75.4 days, meaning that the time between

two consecutive minima (37.7 days) is close to the period of ℓ Car (35.6 days). However, it is clearly less massive, as Bono et al. (1997) give a probable mass below 1 $M_\odot$ for AC Her, compared to $M_{\ell\mathrm{Car}} \approx 13\,M_\odot$ (Caputo et al. 2005). In addition, AC Her was confirmed to be a binary star with a separation of 1.4 AU by Van Winckel et al. (1998) from radial velocity data. These authors also deduce an effective temperature of 5500 ± 250 K for the primary, comparable to ℓ Car ($\simeq$5100 K). AC Her also presents a very strong millimetric continuum flux (Van der Veen et al. 1994) that indicates the presence of large dust grains. Its spectrum shows a clear infrared excess in the N band, including a strong silicate emission feature between 8 and 12 μm (see e.g. Molster et al. 2002). Jura et al. (2000) have obtained mid-IR adaptive optics images of AC Her and detected two compact sources separated by 0.6″. These authors conclude that the best model to explain these observations is an edge-on ring of dust with a radius of 300 AU. However, this result was not confirmed by Close et al. (2003), who exclude any extended emission from high Strehl ratio AO images in the mid-IR domain. Exploring longer wavelengths, De Ruyter et al. (2005) have considered the spectral energy distribution of six bright RV Tau stars up to the millimetric domain in order to characterize the properties of the circumstellar dust. In the case of AC Her, they obtain a best-fit dust model consisting of a shell with an inner radius of 50 $R_\star$ and an external radius of 900 $R_\star$, and a total mass of the order of $3 \times 10^{-5}\,M_\odot$.

While ℓ Car does not present the same infrared excess as AC Her, and is significantly more massive, its physical properties place it at an interesting location in the H−R diagram close to the dusty pulsating RV Tau stars. By analogy with this class of stars, a significant millimetric excess could be present in the spectrum of ℓ Car. Unfortunately, to our knowledge, there are no millimetric observation of this star (or of any classical Cepheid) in the literature.

5.2. Mira stars and red supergiants

Recent observations making use of interferometers and combined with spectroscopic data have shed new light on the atmospheric structure of Miras and red supergiants, and on the interplay between atmospheric structure and dust formation. It is therefore interesting to compare Cepheids to these stars.

Cepheids and Miras undergo regular and large amplitude pulsations with comparable photospheric velocities of a few 10 km s^{-1}. Pulsations are efficient to expand the atmospheric volume and increase the scale height, making the atmosphere of these stars much more extended than for static objects.

Pulsations are mandatory in our current understanding of these objects to levitate material high enough in the atmosphere to allow for dust to condensate and drive the mass loss. Cepheids, as yellow supergiants, are very luminous and naturally have extended atmospheres. The driving mechanism for mass loss in red supergiants could be the production of acoustic energy by large convective cells as supported by Josselin & Plez (2003). Because they pulsate and they are supergiants, Cepheids can potentially use the two mechanisms to lose mass: pulsation and convection.

Perrin et al. (2004a,b, 2005a) have shown that the structure of the atmosphere of Mira stars and of the red supergiants Betelgeuse and μ Cep share some similarities. In both cases, a warm molecular layer with H_2O and CO was described at a short distance from the photosphere, at about 2 $R_\star$ for Mira stars and 1.4 $R_\star$ for red supergiants. The temperatures are also quite similar, of the order of 2000 K. Simultaneous modeling of interferometric and spectroscopic data by Weiner (2004) and Ohnaka (2004b) for Mira stars and by Ohnaka (2004a) for red supergiants confirmed the presence of water vapor in the molecular layer. Recently, Verhoelst et al. (2005) have shown that a consistent view of both interferometric and spectroscopic data of Betelgeuse requires the presence of corondum in the layer, thus providing a seed for silicate dust nucleation. A similar structure could exist around ℓ Car.

As a simple experiment, the properties of the CSE of ℓ Car can be extrapolated to that of Betelgeuse. Assuming thermal equilibrium in the atmosphere of Betelgeuse and assigning a fixed and common distance to all molecules in the atmosphere, a radial temperature law can be derived. The photosphere radiates a flux proportional to $R_\star^2\,T_\star^2$ of which a fraction $\mathrm{e}^{-\tau_l}$ is absorbed by the layer. As a very crude approximation it is assumed that τ_l does not vary with wavelength. Because of thermal equilibrium, the layer radiates a flux proportional to $(1-\mathrm{e}^{-\tau_l})\,R_\mathrm{l}^2\,T_\mathrm{l}^2$. Equating parameters to the values derived in Perrin et al. (2004a) yields $\tau_\mathrm{l} = 1.94$. Using this same optical depth for a hypothetical layer around ℓ Car yields a distance at which the temperature drops to 2000 K of 3.1 $R_\star$. Should the atmospheric contents detected with the interferometric K and N band measurements be water vapor, temperatures of 2000 K or less are required to produce a significant opacity. This simple experiment shows that the parameters derived in this paper for the CSE of ℓ Car a priori make sense physically, and are likely to be in agreement with what could be a general scheme for evolved stars.

One may now wonder at what characteristic distance sillicate dust could condensate, i.e. at what distance does the temperature drop below 1000 K. With the same rationale on thermal equilibrium and assigning an optical depth of 1 to the dust layer, the dust condensation radius order of magnitude is 21 $R_\star$, corresponding to 30 mas at the distance of ℓ Car. Given the resolution of MIDI during the observation, such a structure should have been detected if it exists. The current observations thus point towards a rather poor dusty environment around ℓ Car, a conclusion compatible with the absence of an infrared excess for the star.

6. Conclusion

Based on combined observations in the near and mid infrared domains with the VINCI and MIDI instruments of the VLTI, we have detected a circumstellar envelope around the massive Cepheid ℓ Car. Its typical size is 2−3 $R_\star$, and its contribution to the total near-infrared flux is 4%. Extended dusty environments are known to be present around other types of variable stars related to Cepheids that are located near ℓ Car in the Hertzsprung-Russell diagram. The physical process that created the CSE could be linked to the relatively large mass loss rate of ℓ Car

that could be enhanced by pulsation and convection. Although our data are still insufficient to study the nature of this CSE, a molecular layer could be a plausible explanation for our observations, by analogy with red supergiants and Miras.

Acknowledgements. Based on observations collected with the VLT Interferometer, Cerro Paranal, Chile, in the framework of the ESO programmes 071.D-0425 and 073.D-0142. This research has made use of the SIMBAD database at CDS, Strasbourg (France).

References

Baade, W. 1926, Astron. Nachr., 228, 359
Bastien, P., Drissen, L., Ménard, F., et al. 1988, AJ, 95, 900
Böhm-Vitense, E., & Love, S. G. 1994, ApJ, 420, 201
Bono, G., Caputo, F., & Santolamazza, P. 1997, A&A, 317, 171
Bordé, P., Coudé du Foresto, V., Chagnon, G., & Perrin, G. 2002, A&A, 393, 183
Caputo, F., Bono, G., Fiorentino, G., Marconi, M., & Musella, I. 2005, ApJ, 629, 1021
Claret, A. 2000, A&A, 363, 1081
Claret, A., Diaz-Cordovez, J., & Gimenez, A. 1995, A&AS, 114, 247
Close, L. M., Biller, B., Hoffmann, W. F., et al. 2003, ApJ, 598, L35
Cohen, M., Walker, R. G., et al. 1999, AJ, 117, 1864
Davis, J., Tango, W. J., & Booth, A. J. 2000, MNRAS, 318, 387
Deasy, H. P. 1988, MNRAS, 231, 673
De Ruyter, S., Van Winckel, H., Dominik, C., Waters, L. B. F. M., & Dejonghe, H. 2005, A&A, 435, 161
Di Folco, E., Thévenin, F., Kervella, P., et al. 2004, A&A, 426, 601
Fernie, J. D. 1990, ApJS, 72, 153
Gherz, R. D. 1972, ApJ, 178, 715
Glindemann, A., Albertsen, M., Andolfato, L., et al. 2004, SPIE, 5491, 447
Guyon, O. 2002, A&A, 387, 366
Josselin, É., & Plez, B. 2003, SF2A
Hanbury Brown, R., Davis, J., Lake, R. J. W., & Thompson, R. J. 1974, MNRAS, 167, 475
Havlen, R. J. 1972, A&A, 16, 257
Heiles, C. 2000, ApJ, 119, 923
Jura, M. 1986, ApJ, 309, 732
Jura, M., Chen, C., & Werner, M. W. 2000, ApJ, 541, 264
Kervella, P., Coudé du Foresto, V., Glindemann, A., & Hofmann, R. 2000, SPIE, 4006, 31
Kervella, P., Gitton, Ph., Ségransan, D., et al. 2003, SPIE, 4838, 858
Kervella, P., Ségransan, D., & Coudé du Foresto, V. 2004a, A&A, 425, 1161
Kervella, P., Nardetto, N., Bersier, D., Mourard, D., & Coudé du Foresto, V. 2004b, A&A, 416, 941 (Paper I)
Kervella, P., Fouqué, P., Storm, J., et al. 2004c, ApJ, 604, L113
Kholopov, P. N., Samus, N. N., Frolov, M. S., et al. 1998, Combined General Catalogue of Variable Stars, 4.1 edition (GCVS)
Kiss, L. L., & Szàtmary, K. 1998, MNRAS, 300, 616
Lord, S. 1992, NASA Tech. Mem., 103957
Marengo, M., Sasselov, D. D., Karovska, M., & Papaliolios, C. 2002, ApJ, 567, 1131
Marengo, M., Karovska, M., Sasselov, D. D., et al. 2003, ApJ, 589, 968
McAlary, C. W., & Welch, D. L. 1986, AJ, 91, 1209
Molster, F. J., Waters, L. B. F. M., & Tielens, A. G. G. M. 2002, A&A, 382, 222
Moskalik, P., & Buchler, J. R. 1991, ApJ, 366, 300
Ohnaka, K. 2004a, A&A, 421, 1149
Ohnaka, K. 2004b, A&A, 424, 1011
Perryman, M. A. C., Lindegren, L., Kovalevsky, J., et al., The HIPPARCOS Catalogue 1997, A&A, 323, 49
Perrin, G., et al., in preparation
Perrin, G., Ridgway, S. T., Mennesson, B., et al. 2004, A&A, 426, 279
Perrin, G., Ridgway, S. T., Verhoelst, T., et al. 2005, A&A, 436, 317
Perrin, G., Ridgway, S. T., Coudé du Foresto, V., et al. 2004, A&A, 418, 675
Petrov, R., Malbet, F., Richichi, A., et al. 2000, SPIE, 4006, 68
Polyakova, T. A. 1990, Pis'ma Astron. Zh., 16, 916
Serkowski, K., Mathewson, D. S., & Ford, V. L. 1975, ApJ, 196, 261
Shenton, M., Albinson, J. S., Barrett, P., et al. 1992, A&A, 262, 138
Szabados, L. 1989, Commmunications of the Konkoly Observatory Hungary, 94, 1
Szabados, L. 2003, Comm. Konkoly Obs., 103, 115
Taylor, M. M., Albrow, M. D., Booth, A. J., & Cottrell, P. L. 1997, MNRAS, 292, 662
Van der Veen, W. E. C. J., Waters, L. B. F. M., Trams, N. R., & Matthews, H. E. 1994, A&A, 285, 551
Van Winckel, H., Waelkens, C., Waters, L. B. F. M., et al. 1998, A&A, 336, L17
Verhoelst, T., Decin, L., Van Malderen, R., et al. 2005, A&A, submitted
Volk, K., & Cohen, M. 1989, AJ, 98, 1918
Wallerstein, G. 2004, PASP, 114, 689
Weiner, J. 2004, ApJ, 611, L37
Wesselink, A. 1946, Bull. Astron. Inst. Netherlands, 10, 91
Willson, L. A. 1988, Pulsation and Mass loss in Stars (Kluwer), 285